Title

Fluid saturation and pressure prediction in a multi-component reservoir by combined seismic and electromagnetic imaging

Authors

Hoversten, G. Michael
Gritto, Roland
Washbourne, John
et al.

Publication Date

2002-06-10

Fluid saturation and pressure prediction in a multi-component reservoir by combined seismic and electromagnetic imaging

G. Michael Hoversten*, Roland Gritto, Lawrence Berkeley National Laboratory, John Washbourne, TomoSeis Inc. and, Tom Daily, Lawrence Berkeley National Laboratory

Summary

The quantitative estimation of changes in water saturation (S_w) and effective pressure (P) in terms of changes in compressional and shear impedance is becoming routine in the interpretations of time-lapse surface seismic data. However, when the number of reservoir constituents increases to include in situ gas and injected CO_2 there are too many parameters to be determined from seismic velocities or impedances alone. In such situations the incorporation of electromagnetic (EM) images of the change of electrical conductivity (σ) provides essential independent information. The purpose of this study was to demonstrate a methodology for jointly interpreting cross well seismic and EM data in conjunction with detailed constituative relations between geophysical and reservoir parameters to quantitatively predict changes in P, S_w, gas saturation (S_g) and gas/oil ratio (R_g) in a reservoir undergoing CO_2 flood.

Introduction

Crosswell seismic and EM technology has been developed over the past two decades to provide high spatial resolution images of the compressional velocity (V_p), shear velocity (V_s) and the σ of the inter-well region. The majority of effort, as measured by the topics of published and presented work, has concentrated on developing and improving algorithms for estimating the geophysical parameters themselves. In most reported applications the output from a survey is a cross section of V_p, V_s or σ or the time-lapse change (Δ) of these parameters, which is discussed in terms of its implications for the distribution and/or Δ of the reservoir parameter of interest. These interpretations are qualitative and can be in error when more than one reservoir parameter effects the geophysical parameter.

Simple regression fits between V_p and S_w, for example, can be used to convert from geophysical to reservoir parameters. This approach can be used successfully in relatively simple environments with a minimum of fluid components. However, in many settings the geophysical parameters depend on many reservoir parameters that are variable in both space and time. In particular ϕ, P, S_w and S_g strongly influence V_p. σ can generally be described as a function of ϕ, S_w and fluid σ (Archie 1942). As we will show in a multi-component fluid reservoir the spatial distribution of the time-lapse change in geophysical parameters, such as V_p, can vary significantly from the spatial distribution of the time-lapse change in a desired reservoir parameter such as S_g. This is due to the geophysical parameters dependence on other parameters such as P and S_w that must be sorted out before a picture of any single reservoir parameter can be obtained.

The objective of the work described in this paper is to demonstrate a methodology of combining time-lapse changes in σ, V_p and V_s with a detailed rock properties model to produce quantitative estimates of the change in fluid saturations (including oil, water and gas) and reservoir pressure.

Experiment Description

Crosswell seismic and EM measurements were conducted in the Lost Hills oil field in southern California during a CO_2 injection pilot study conducted by Chevron Petroleum Co. The P and T of the reservoir make this an immiscible flood; CO_2 is in the gas phase within the reservoir. The experiment took place in a portion of the field that had been undergoing water flood since 1995. Figure 1 shows the placement of relevant wells and estimated hydrolic fracture locations.

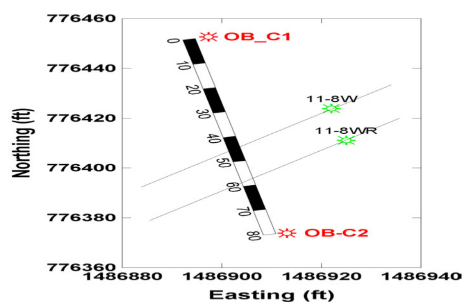

Figure 1: Plan view of observation wells OB-C1 and OB-C2 with old water injector 11-8W and new CO_2 injector 11-8WR. Estimated hydrolic fracture locations are shown as black lines.

The observation wells, OB-C1 and OB-C2, were drilled for the pilot and fiberglass cased to allow the use of crosswell EM. The nearby CO_2 injector (11-8WR) is located just 20 feet out of the crosswell-imaging plane. The injection wells are hydraulically fractured to increase injectivity into the low permeability Diatomite reservoir. In some cases down hole pressures were increased above the lithostatic pressure, which may have induced fracturing above the desired injection interval. If the fracture did indeed extend above the desired interval there is a high probability that much of the injected

CO_2 will not sweep its intended target but will move in the higher section.

The base line crosswell seismic and EM surveys were conducted in September 2000 just prior to the beginning of CO_2 injection. Two seismic sources were used; a piezoelectric V_p source and an orbital vibrator V_s source with maximum frequency contents of 2000 and 350 Hz respectively. A repeat seismic survey was conducted in late May 2001 with the repeat EM survey conducted in early July 2001.

A rock properties model

The reservoir parameters that have a dominant affect on the geophysical parameters are ϕ, P, S_w and S_g. Effective pressure, P, is equal to lithostatic minus pore pressure (P_{pore}). So as P_{pore} increases, P will decrease. Pressure has a significant effect in Lost Hills since this is a shallow reservoir in soft rock. We sought constituative relations between geophysical and reservoir parameters (rock properties model) that would be able to predict observed V_p, density and σ from observed P, ϕ, S_w and S_g. Laboratory measurements of the dry frame moduli and grain density of the Diatomite reservoir rock were

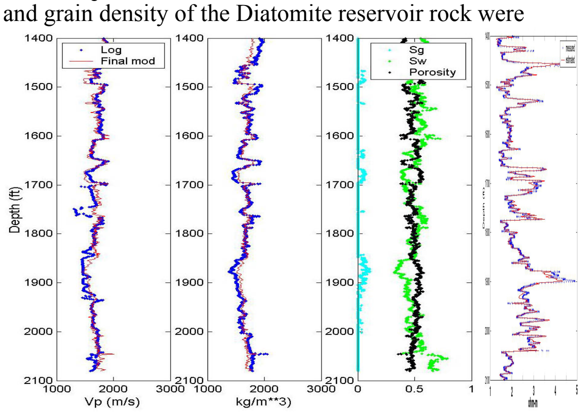

Figure 2: Rock properties model uses logged porosity (black), water saturation (green) and gas saturation (light blue) as inputs in a multi-parameter simplex regression to predict the V_p (left panel), density (second from left panel) and electrical resistivity (right panel). Measured V_p, density and resistivity are shown in blue, model predicted values shown in red.

unavailable so Hertz-Mindlin theory with the modified Hashin-Strikman lower bound (Hashin & Shtrikman 1963) was used to model the dry frame moduli of the reservoir rock. Fluid substitution in the dry frame is modeled by Gassmann's equation. The bulk modului and densities of gas, live oil and brine as well as the gas/oil ratio (R_g) are modeled using relations published by Betzel and Wang (1992). The bulk σ of the reservoir rock is modeled using Archie's (1942) relationship.

A simplex algorithm was used to solve for the model parameters that would minimize the combined miss-fit between observed V_p and density logs and the model predictions given the ϕ, S_w and S_g logs. Because the wells did not have full logging suites a nearby well with a full suite of logs was used. The results of this minimization along with the Archie's law fit to the OBC1 σ log are shown in Figure 2.

The pressure prediction capability of the model was validated by comparison to measurements made by Wang (2001) on core samples of Diatomite from the Lost Hills field. Figure 3 presents the measured data recast as ΔV_p as a function of ΔP about a reference P of 4.7 MPa, the effective pressure in the reservoir at the start of CO_2 injection.

For expected decreases in P in the range 0 to 2.5 MPa from the initial pressure the model predictions are within a few percent of the lab measurements for vertical V_p.

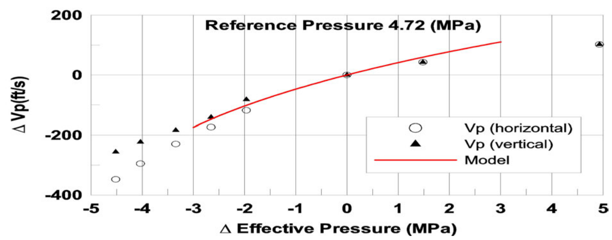

Figure 3: Predicted V_p change as a function of change in effective P compared to laboratory measurements on Lost Hills diatomite core samples.

The rock properties model is used to calculate changes in V_p, V_s and σ as functions of changes in P, S_w, S_g and S_{CO2} when certain reference values of P, ϕ, S_w and S_g are assumed. Figure 4 shows ΔV_p and ΔV_s as functions of ΔP and ΔS_w about a

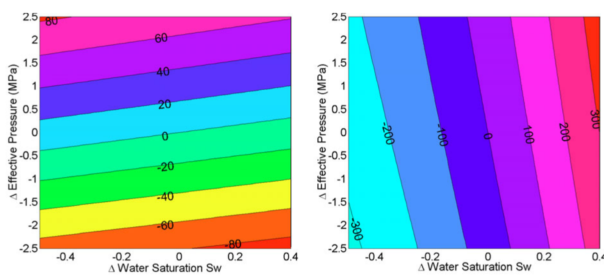

Figure 4: ΔV_s (left panel) and ΔV_p (right panel) vs. ΔP and ΔS_w about a reference S_w, S_g, ϕ and P of 0.5, 0.0, 0.5 and 4.7 MPa.

reference point (reservoir just prior to CO_2 injection) where S_w, S_g, ϕ and P and equal 0.5, 0.0, 0.5 and 4.7 (MPa) respectively. Relations between ΔV_p and ΔV_s and ΔP and ΔS_w such as illustrated in Figure 4 form the basis of 4D seismic ΔP and ΔS_w prediction. However, when S_g is non-zero as shown in Figure 5, the orientation and magnitude of contours of constant ΔV_p change dramatically. ΔV_s is only slightly effected (through density) by the presence of gas. Without additional information ΔV_p and ΔV_s are insufficient to

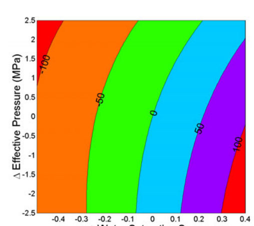

Figure 5: ΔV_p at Sg=0.05

predict ΔP, ΔS_w and ΔS_g. EM data provides an independent estimate of ΔS_w. σ is a much simpler function of reservoir parameters than is the velocity and can be described by Archie's law (Archie 1942). Assuming ϕ is constant $\Delta\sigma$ is only a function of ΔS_w and Δ pore σ. Since water flood has been in effect for over 6 years we assume that the pore fluid water has reached equilibrium between injected and native water and fluid σ does not change. Therefore, conductivity changes are interpreted solely in terms of water saturation changes.

Integrated time-lapse geophysical images

The strategy we adopted to maximize the spatial correlation between V_p, V_s and σ images was to begin with the EM were the most a priori information existed and then use the σ images to produce starting V_p models followed by producing starting V_s models from the final V_p models. We chose to use a conjugate gradient algorithm (Jackson & Tweeton 1996) because the final model is sensitive to the initial model and is perturbed from the starting values only as much as needed to fit the observed data.

The EM inversion (Newman 1995) for the data at initial conditions was started from a model built by laterally interpolating the σ logs between the OB-C1 and OB-C2 wells. The EM inverse σ model at initial conditions was then used as the starting model for the inversion of the July 2001 EM data. Differencing these inversions provides the $\Delta\sigma$ shown in Figure 6c. There is a high degree of correlation between the 11-8WR permeability log and the areas where the largest decrease in σ occur. The correlation between high permeability and large changes in S_w, and thus σ, is expected. Also, the largest σ changes occur more in alignment with the estimated location of the old water injection fracture than with the much newer CO_2 fracture. This is not surprising when we consider that the water injection was ongoing for more that 6 years and thus likely produced a high permeability damage zone that is a better conduit to flow than the very new CO_2 fracture.

Next the pre and post CO_2 σ models were converted to V_p, these were then used as initial models in the inversion of the V_p travel time data to produce the change in V_p shown in Figure 6b. In addition to V_p changes occurring in the vicinity of the estimated water injection fracture there are decreases in V_p that align with the mapped fault. Since there are little σ changes associated with the fault we interpret this to mean that pressure changes are occurring along the fault zone without significant changes in water saturation.

The V_p sections were converted to V_s using a V_p/V_s ratio derived from the rock properties model and used as starting models for the V_s travel time inversions resulting in the ΔV_s section shown in Figure 6a. The ΔV_s section is smoother than either the $\Delta\sigma$ or ΔV_p sections due in part to the lower frequency content in the shear wave data. The ΔV_s section is also smoother because Vs is relatively insensitive to ΔS_w that has high spatial variability but very sensitive to ΔP that has much lower spatial variability. Even with the smoother spatial changes in the V_s data we see correlation with the V_p and σ changes. In particular the zone along the fault shows a decrease in V_s, lending support to our interpretation that pressure is changing along the fault zone.

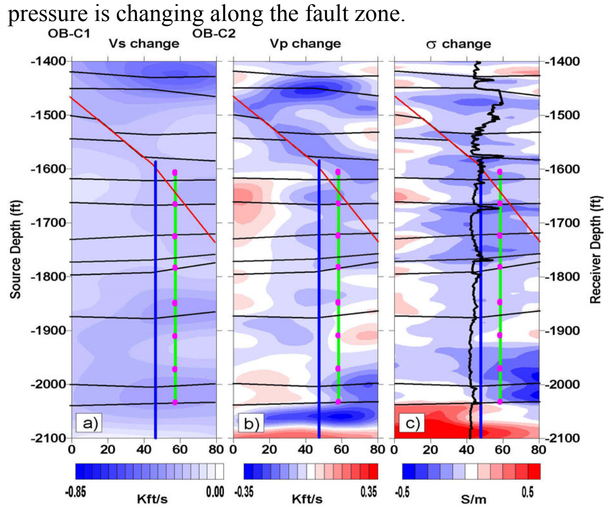

Figure 6: Time-lapse changes in a) V_s, b) V_p and c) σ. Major unit boundaries are shown as black horizontal lines, estimated location of previous water injection fracture is shown as vertical blue line (x=45ft), estimated location of the CO_2 injection fracture is shown as a vertical green line (x=60ft), perforation intervals for CO_2 injection are shown as magenta dots, location of a fault zone is shown as the red diagonal line. The permeability log from the CO_2 injection well 11-8WR is shown in black on panel c).

Predicting changes in reservoir parameters

First the $\Delta\sigma$ image was used to predict ΔS_w assuming that ϕ and fluid σ did not change. The predicted ΔS_w was used with the observed ΔV_s and the relation illustrated in Figure 4a to predict ΔP. The predicted ΔS_w and ΔP were then used to calculate the ΔV_p that would be due to ΔS_w and ΔP alone assuming S_g=0. Over the majority of the image plane ΔS_w and ΔP are negative thus producing a negative ΔV_p. The difference between the observed and calculated ΔV_p (ΔV_R) was generated. We expect the CO_2 to decrease V_p in excess of the effects of ΔS_w and ΔP alone. There are two mechanisms for CO_2 to decrease V_p; 1) through decreasing the bulk modulus of the oil by increasing the gas/oil ratio and 2) by increasing S_g through introduction of free CO_2. Either of these mechanisms would produce a negative ΔV_R. On the other hand, if ΔV_R is positive this indicates that ΔV_p calculated from ΔS_w and ΔP assuming S_g=0 is too large. The presence of initial gas will produce this effect, as seen in Figure 5 where the presence of gas reduces the decrease in V_p associated with a given ΔS_w and ΔP.

The OB-C1 log shows the presence of gas over certain intervals within the reservoir. Therefore a two-step process was used to calculate ΔV_R. The first pass used S_g=0 as described. Next, sections of the image where ΔV_R was positive were recalculated assuming S_g = 0.05 (the average non-zero S_g in the reservoir interval). After the second pass calculation of ΔV_R much of the areas that had $+\Delta V_R$ after pass one became negative. The final ΔV_R was converted to ΔR_g and ΔS_g where both CO_2 and hydrocarbon gas are considered.

This final step requires assumptions about the partitioning of -ΔV_R. First we assumed that the $+\Delta P_{pore}$ caused by injection would drive as much of the initial S_g into the oil as possible. Next we assume a partitioning between the $+\Delta R_g$ and $+\Delta S_{CO2}$ effects on ΔV_R. We chose to allow the maximum increase in CO_2 R_g for the given $+\Delta P_{pore}$. -ΔV_R was converted to $+\Delta R_g$ up to the maximum R_g for the final P_{pore} and T. If the $+\Delta R_g$ did not completely account for the -ΔV_R, then ΔS_{CO2} was calculated to account for the rest. Figure 7 shows the calculated ΔR_g and ΔS_g generated from the geophysical parameter changes shown in Figure 6. As has been stated these calculations are based on differences calculated about reference values of P, ϕ, S_w and S_g. The sensitivity of the ΔR_g and ΔS_g predictions to the reference parameters has been studies and shows that the calculations are relatively insensitive to the reference ϕ and S_w values. The calculations are most sensitive to the reference P.

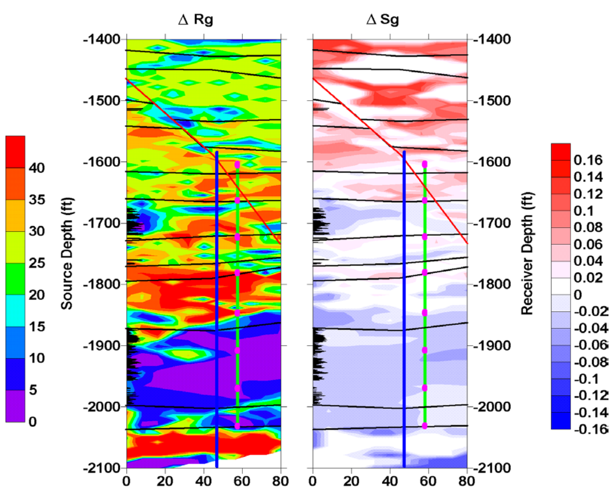

Figure 7: Predicted ΔR_g (left side) and ΔS_g (right side). Initial OB-C1 gas log in black on left side. See Figure 6 caption for figure overlays.

P from a history matched flow simulation model at the beginning of CO_2 injection was used as a reference to produce the results shown in Figure 7. The effect of the reference P can be seen above 1600 ft where there is a large $+\Delta S_g$ and relatively low $+\Delta R_g$. This is due to the relatively low initial P_{pore} in this region, which reduces the amount of gas (CO_2 or hydrocarbon) that can dissolve in the oil as P_{pore} increases. The effect of changing the reference P to a constant, such as the average before injection, is to cause a larger $+\Delta R_g$ and a smaller $+\Delta S_g$ in the upper section. The effect of the reference P below 1600ft is negligible.

There is a strong correlation between the areas with initial gas, as indicated by the gas log (left side of Figure 7), and areas with high -ΔS_g and low $+\Delta R_g$. This is consistent with the initial gas in place being driven into the oil with $+\Delta P_{pore}$ thus reducing the amount of CO_2 that can be dissolved in the oil. In addition, the images of ΔS_g and ΔR_g have a much higher spatial correlation with unit boundaries and the fault zone than do the individual time-lapse geophysical images. This is a benefit of partitioning the geophysical changes by first removing the effects of ΔP and ΔS_w.

Conclusion

We have demonstrated that by combining seismically derived ΔV_p and ΔV_s with EM derived $\Delta\sigma$ estimates of ΔP, ΔS_w ΔS_g and ΔR_g can be made in a complex reservoir containing oil, water, hydrocarbon gas and introduced CO_2. The resulting predicted ΔS_g and ΔR_g are better correlated with logged unit boundaries than are any of the Δ geophysical parameter images. The predicted ΔS_g and ΔR_g images indicate that a significant portion of the injected CO_2 is filling the upper portions of the section above the intended injection interval. These conclusions are validated by CO_2 injectivity measurements made in the 11-8WR well.

While the methodology outlined in this paper relies on many assumptions that were required because the project was not designed to use this methodology in future applications these could be substantially reduced by design. In particular, the most benefit could be drawn from repeat logging of the wells with a full suite of logs. This would provide control points for the ΔP, ΔS_w, ΔS_g, ΔV_p, ΔV_s and $\Delta\sigma$ all of which would serve to greatly constrain the problem. In addition, having full log suites would enable much better control of the geophysical inverse solutions through superior starting models.

References

Archie, G. E., 1942, The electrical resistivity log as an aid in determining some reservoir characteristics. Trans. Am. Inst. Mech. Eng., 146, 54-62.

Betzel, M. and Wang, Z., 1992, Seismic properties of pore fluids, Geophys., 57, 1396-1408.

Hashin, Z., and Shtrikman, S., 1963, A variational approach to the elastic behavior of multiphse materials, J. Mech. Phys. Solids, 11, 127 – 140.

Newman, G. A., 1995, Crosswell electromagnetic inversion using integral and differential Equations: Geophysics, **60**, 899-911.

Jackson, M. J. and Tweeton, D. R., 1996, 3DTOM: Three-Dimensional Geophysical Tomography, US Dept. of the Interior, Bureau of Mines, Report of Investigation 9617.

Wang, Z., 2001 Personal Communication